© IWA Publishing 2020
130

Water Practice & Technology Vol 15 No 1
doi: 10.2166/wpt.2020.003

Lead and cadmium removal by adsorption process using hydroxyapatite porous materials

Amina Ramdani[a,*], Abdelkader Kadeche[a], Mehdi Adjdir[b], Zoubida Taleb[c], Djamila Ikhou[a], Safia Taleb[c] and André Deratani[d]

[a] Department of Chemistry, Faculty of Sciences, University Dr. Moulay Tahar, Saida 20000, Algeria

[b] Department of Engineering Process, Faculty of Technology, University Dr. Moulay Tahar, Saida 20000, Algeria

[c] Laboratory of Materials & Catalysis, Faculty of Exact Sciences, Djillali Liabès University, Site I, B.P. 89, Sidi Bel-Abbès 22000, Algeria

[d] IEMIUM2, Place Eugène Bataillon, Case Courrier 047, 34095 Montpellier Cedex 5, France

*Corresponding author. E-mail: ramdaniamina010@gmail.com

Abstract

This contribution is a comparison study between synthetic hydroxyapatite (Sy-HAP) and commercial hydroxyapatite (C-HAP) for the removal of Pb^{2+} and Cd^{2+} ions present in wastewater from industrial effluents. The obtained results show that the equilibrium time required for complete adsorption of Pb^{2+} and Cd^{2+} ions on C-HAP and Sy-HAP is 15 min for both. The obtained removal efficiencies for Sy-HAP are 95.52% and 90.91% for Pb^{2+} and Cd^{2+} ions, respectively. Whereas, C-Hap presents lower removal efficiencies of 86.53% and 81.43% for Pb^{2+} and Cd^{2+} ions, respectively. Maximum adsorption was observed at pH 5; at lower pH levels adsorption was less. The experimental kinetic data fitted with the second order kinetic model. Thermodynamically, the adsorption process was endothermic and spontaneous in nature. Isotherm adsorption studies indicated that Langmuir, Freundlich and Temkin are the most valid models to describe and evaluate the adsorption process. The EDX results also confirmed the presence of lead and cadmium in adsorbents after adsorption. Finally, the HAP porous materials possess great potential for the removal of Pb^{2+} and Cd^{2+} ions from aqueous solutions and wastewater from industrial effluents.

Key words: adsorption, heavy metals, porous hydroxyapatite, wastewater

INTRODUCTION

Water pollution has a major ecological impact on the environment and human health usually due to industrial effluents with toxic substances such as heavy metals (Lu *et al.* 2014). Many researches are focused on lead (Pb) and cadmium (Cd) ions which are *extremely* toxic at low concentrations and considered as carcinogenic heavy metals (Sönmezay *et al.* 2012). These heavy metals are poured into water and groundwater from mining and petrochemicals industries (Li *et al.* 2019). Therefore, numerous approaches such as chemical precipitation, adsorption, membrane process, and electrochemical treatment have been investigated to improve and purify the quality of water by reducing the concentration of heavy metals in wastewater (Mousa *et al.* 2016; Jing *et al.* 2018). Governments and environmental protection agencies fixed the limit values and guidelines recommended in terms of the allowable concentration for lead and cadmium in wastewaters from industrial effluents and drinking water. The permissible limits recommended by World health Organization (WHO 1993) are 0.01 mg/L and 0.003 mg/L for Pb^{2+} and Cd^{2+} ions respectively. Also, Algeria sets a regulatory

Water Practice & Technology Vol 15 No 1
doi: 10.2166/wpt.2020.003

framework, which considers lead and cadmium as toxic products and shows that the limit values must not exceed 0.01 mg/L (for Pb^{2+}) and 0.003 mg/L (for Cd^{2+}) for drinking water (Official Journal of the Algerian Republic 2006), and 0.5 mg/L (for Pb^{2+}) and 0.2 mg/L (for Cd^{2+}) for discharge in sewage (Official Journal of the Algerian Republic N°18 2011).

Many attempts have been made by researchers for the removal of heavy metals using mesoporous materials, and nanoporous particles such as zeolites, polymers, organic resins, silicate, clays, carbon nanotubes and apatites (Ullah *et al.* 2016; Song *et al.* 2016; Alexander *et al.* 2017; França de Oliveira *et al.* 2017; Kołodyńska *et al.* 2017; Pobi *et al.* 2019). The latter has shown remarkable heavy metal efficiencies. Hydroxyapatite (Ca_{10} $(PO_4)_6$ $(OH)_2$) belongs to the crystallographic family of apatite with a hexagonal structure under Ca/P ratio between 1.67 and 1.5 (Song *et al.* 2016). Hydroxyapatite (Hap) is a natural important mineral that consists mainly of calcium and phosphate (Kemençe & Bölgen 2017) and can be found in human and animal hard tissues like vertebrate bones, mammalian teeth, fish scales, and the mature teeth of some chiton species (Zhao *et al.* 2012). Because of its abundance and low cost, hydroxyapatite (Hap) is attracting interest in biology, chemistry and in medical biomaterial such as implants for its chemical composition similarity to the natural bone (Zhao *et al.* 2012). Hydroxyapatite (Hap) can be synthesized and prepared via several methods, such as electro-deposition or sol-gel method (wet-chemical precipitation) (Ben-Arfa *et al.* 2017). Hydroxyapatite is one of the promising materials because of its high specific surface area, and high adsorption ability in drug delivery (Yan *et al.* 2016) dyes and proteins adsorption (Kim *et al.* 2016), and in particular removal of heavy metal ions from wastewater (Sönmezay *et al.* 2012). This research focuses on the synthesis of hydroxyapatite (Sy-Hap) from bovine bone as a low-cost and effective crystalline adsorbent, as well as a comparative study of the heavy metals removal efficiency between hydroxyapatite (Sy-HAP) and commercial (C-HAP).

MATERIALS AND METHODS

Reagents and apparatus

Reagents and chemicals used in this study were of analytical grade $Pb(NO_3)_2$, $Cd(NO_3)_2$, and commercial Hydroxyapatite was purchased from Sigma Aldrich. HNO_3 and NaOH were purchased from Biochem. Stock solutions of Pb^{2+} and Cd^{2+} ions were prepared with concentration of 10^{-2} mol/L by dissolving 3.318 g and 3.054 g of Pb $(NO_3)_2$ and Cd $(NO_3)_2$ salts respectively in demonized water (1,000 mg/L). The Pb and Cd ion concentrations were measured using a UV–Visible Spectrophotometer (UV-UV-2401PC of Schimadzu mark) at wavelengths of 650 nm and 600 nm respectively, according to a procedure described elsewhere (Murakami 1981).

The porous texture and the specific surface area of the samples were determined by nitrogen physisorption at 77 K, using a Micromeritics ASAP 2000 volumetric adsorption device after sample out-gassing at 383 K under vacuum for 4 h. The specific surface area (SBET) of both samples was obtained by adopting the BET equation (Brunauer-Emmett-Teller). The microporous and mesoporous volumes deduced from the data of the N_2 adsorption-desorption isotherms are calculated respectively, according to the methods of Dubinin-Radushkevich (DR) and Barrett, Joyner and Halenda (BJH). In order to determine the pH_{PZC} of the Hydroxyapatites, we used the methods described in previous studies (Herbache *et al.* 2016).

For SEM observations, the morphological analysis of the adsorbent samples was performed by Scanning Electron Microscopy (SEM), using a Hitachi S-4500 microscope in the secondary electron scanning mode, working at an operation voltage of 30 kV and coupled with an energy dispersive spectrometer (EDS, Thermofisher). The samples were deposited on a wafer containing silver lacquer and metallic gold or carbon. Fourier transform infrared spectroscopy (FTIR) was carried out using a

Water Practice & Technology Vol 15 No 1
doi: 10.2166/wpt.2020.003

Bruker Alpha Model Frontier/Multiscope spectrophotometer over a range of 350–3,800 cm^{-1} with a resolution of 1 cm^{-1}.

Materials

The adsorbents used in this study were synthetic hydroxyapatite (Sy-HAP) from bovine bone and hydroxyapatite (C-HAP), which is a commercially available product as reference. To obtain Sy-HAP, the femur bone of the cow sample was washed with distilled water, hydrogen peroxide, nitric acid and bleach to remove impurities. After that, the cleaned bone was heated in an electric furnace (Nabertherm GmbH-LV9/11 B180 (from 30 °C to 3,000 °C)) under ambient conditions; at 850 °C using a heating rate of 58 C/min with 2 h holding time to remove organic substances and avoid any microbial contamination. Then, the obtained bone ash was dried at 100 °C for six hours. The final product was a white powder indexed as Sy-HAP to be used further for heavy metal removal from wastewater.

Batch adsorption experiments

Adsorption process was performed as a function of contact time, pH, initial metal ion concentrations and temperature in batch mode using adsorbent dosage of 50 mg and adsorbate volume of 100 mL (0.1 L) under determined concentrations. After the equilibrium time was reached, the liquid phase was recovered and filtered. Adsorption equilibrium studies were carried out by varying: the initial metal cation concentrations from 10^{-3} to 10^{-5} M; contact time between solid–liquid were 0–120 min; pH varied from 3 to 7 and temperature was from 25 to 80 °C. The removal percentage (R%) of Pb^{2+} and Cd^{2+} ions was calculated as follows Equation (1):

$$\%\,\text{adsorption} = \frac{(C_i - C_{eq})100}{C_i} \tag{1}$$

where C_i is the initial concentration (mol/L) and C_{eq} is the equilibrium concentration (mol/L).

The amount of heavy metal adsorbed q_e (mg/g) was calculated using the following Equation (2):

$$q_e = \frac{X}{m} = \frac{(C_i - C_{eq})V}{m} \tag{2}$$

where q_e is the amount of heavy metal adsorbed (mg/g), C_i is the initial concentration (mg/L), C_{eq} is the equilibrium concentration (mg/L), V is the volume of the solution (L), m is the mass of adsorbent (g), and X is mass of heavy metal adsorbed (mg).

In order to understand the mechanism and dynamism of adsorption, three kinetic models have been chosen pseudo, first-order (Equation (3)), pseudo second-order (Equation (4)) and intra-particle diffusion (Equation (5)) (Herbache *et al.* 2016):

$$Ln(q_e - q_t) = Ln(q_e) - K_1 t \tag{3}$$

$$\frac{t}{q_t} = \left(\frac{1}{K_2 q_e^2}\right) + \left(\frac{1}{q_e}\right)t \tag{4}$$

Morris and Weber (Xu *et al.* 2017) considered the evolution of the solute concentration in the solid phase depends on $t^{1/2}$.

$$q_t = \frac{X}{m} = K_{diff} t^{\frac{1}{2}} \tag{5}$$

Water Practice & Technology Vol 15 No 1
doi: 10.2166/wpt.2020.003

where q_e and q_t are the amounts of metal ions adsorbed on the hydroxyapatite (mg/g), at equilibrium and at time t respectively and k_1 is the first-order rate constant (min^{-1}). K_2 is the second-order rate constant (g/mg*min).

The experimental results of adsorption were described and analyzed by four isotherm models, i.e. Langmuir, Freundlich, Temkin and Dubinin-Radushkevich (D-R). The Langmuir, Freundlich, Temkin and Dubinin-Radushkevich (D-R) adsorption isotherms can be described by the following relations (Moftakhar *et al.* 2016; Xu *et al.* 2017):

$$\frac{C_{eq}}{q_e} = \frac{1}{K_L q_m} + \frac{C_{eq}}{q_m} \tag{6}$$

$$\text{Ln } q_e = \ln K_F + \frac{1}{n} \ln C_{eq} \tag{7}$$

$$q_e = B_T \ln K_T + B_T \ln C_{eq} \left(B_T = \frac{RT}{b_T} \right) \tag{8}$$

$$\ln q_e = \ln q_{mDR} - K_{DR} \varepsilon^2 \left(\varepsilon = RT \ln \left(1 + \frac{1}{C_{eq}} \right) \right) \tag{9}$$

where q_m, K_L, K_F, n, B_T, b_T, K_T, q_{mDR} and K_{DR} are constants for the above equations (Table 3). The thermodynamic parameters, i.e. the Gibbs free energy (ΔG_{ads}), standard enthalpy (ΔH_{ads}), and entropy (ΔS_{ads}) of adsorption were calculated using the following equations (Lu *et al.* 2014).

$$LnK_d = \frac{\Delta S_{ads}}{R} - \frac{\Delta H_{ads}}{RT} \tag{10}$$

$$\Delta G = \Delta H_{ads} - T \Delta S_{ads} \tag{11}$$

The apparent equilibrium constant (K_d) of adsorption is defined as:

$$K_d = \frac{C_{ads}}{C_{eq}} \tag{12}$$

where R (8.314 J/mol K) is the ideal gas constant.

RESULTS AND DISCUSSION

Characterization

The FTIR spectra of both hydroxyapatites, C-HAP and Sy-HAP, samples are presented in Figure 1. The stretching vibration bands of -OH groups in both hydroxyapatites, C-HAP and Sy-HAP, are found between 3,500 cm^{-1} and 3,570 cm^{-1}. The absorptions at 1,081 cm^{-1} and 1,030 cm^{-1} are attributed to the stretching vibrations of $P=O$. The bands at 570 cm^{-1}, 601 cm^{-1} and 954 cm^{-1} correspond to the bending vibrations of P-O in PO_4^{3-} (Song *et al.* 2016; Jing *et al.* 2018). Moreover, the weak bands located between 1,460 cm^{-1} and 1,415 cm^{-1} are related to the CO_3^{2-}; this band is similar to that found in layered double hydroxide (Cengiz *et al.* 2008). In addition, C-HAP presents a band centered at 1,632 cm^{-1} and assigned to the deformation vibrations of –OH attributed to H_2O molecules physisorbed. Sy-HAP involves two bands stretching and bending located at 1,500 cm^{-1} and 1,650 cm^{-1} attributed to C = O and N-H groups respectively (Cengiz *et al.* 2008). These two bands confirm the existence of organic matter.

Water Practice & Technology Vol 15 No 1
doi: 10.2166/wpt.2020.003

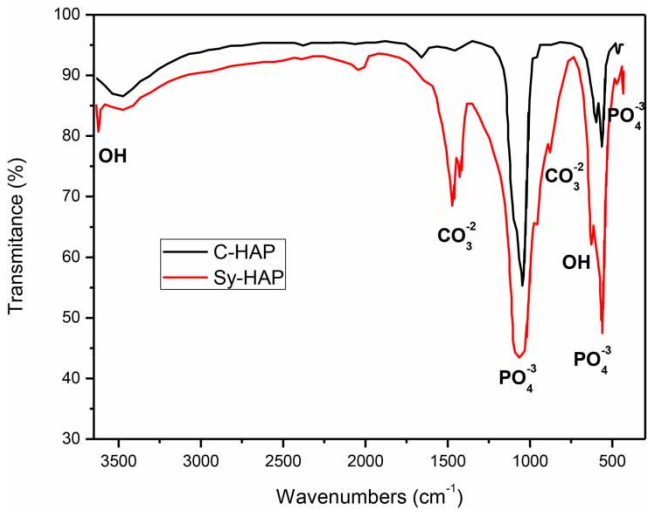

Figure 1 | FTIR spectra of hydroxyapatite Sy-Hap and C-Hap.

The SEM micrographs of the Sy-HAP and C-HAP are given in Figure 2. C-HAP presents aggregation particles with cylindrical rod-like shapes, whose sizes are about 50–100 nm. However, the synthetic hydroxyapatite (Sy-HAP) presents the existence of different size of particles. These latter appear in the form of irregular spheroidal and amorphous grains, which indicated a reduction in crystallinity. Sy-HAP contains multiple pores created by decomposition of organic substances during calcinations at 800 °C (Khoo *et al.* 2015).

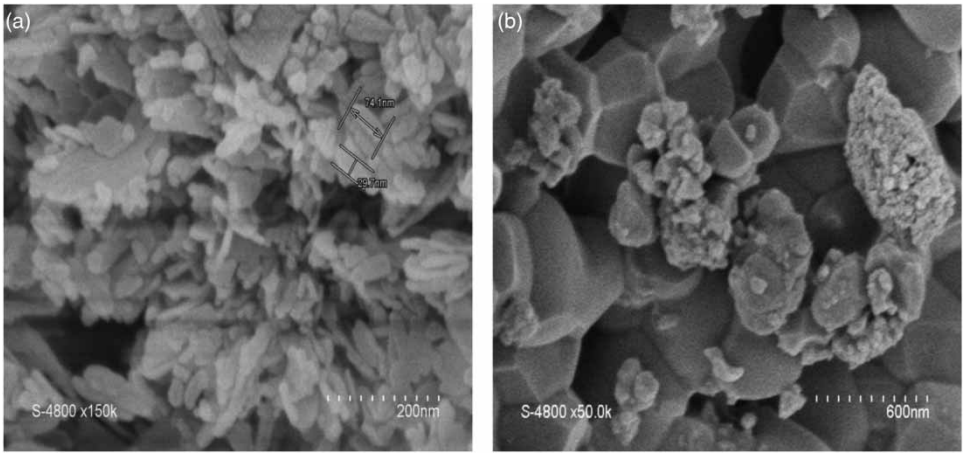

Figure 2 | SEM micrographs of (a) C-Hap and (b) Sy-Hap.

The comparison of the average pore diameter (Dp) is given by two methods, the geometrical one (4Vp/SS) and the BJH. The specific surface area (SS) and the pore volume (Vp) are obtained by the BET method. It can be deduced that the specific surface area of C-HAP and Sy-HAP are 40.8 m^2/g and 46.8 m^2/g respectively. The pore size distribution value of both biomaterials, namely Sy-HAP and C-HAP, calculated by BJH method are 13.9 nm and 25.5 nm respectively. However, by using the geometrical method, it is noticed a pore size distribution decrease for both biomaterials 10.1 nm for Sy-HAP and 24.6 nm for C-HAP respectively. The pore volume of C-HAP is around 0.02 cm^3/g where, Sy-HAP is ca 0.18 cm^3/g. On the basis of these results, it can be noted that both hydroxyapatites Sy-HAP and C-HAP are mesoporous materials. The pH of zero point charge (pHpzc) values of Sy-HAP and C-HAP were found 5.8 and 4.6, respectively.

Water Practice & Technology Vol 15 No 1
doi: 10.2166/wpt.2020.003

After the adsorption of Cd^{2+} and Pb^{2+} ions, the two hydroxyapatites were dried at 80 °C overnight and their chemical compositions were determined by EDX (see data in Figure 3). The Ca/P molar ratio of HAP (1.657) was close to the stoichiometric data of 1.67 (Khoo *et al.* 2015; Jing *et al.* 2018). This result seems to be higher than that of C-HAP. The quantitative elemental analysis given by EDX present in the Sy-HAP and C-HAP samples are C, O, P, Ca, Mg and Na. The presence of oxygen (O), calcium (Ca) and phosphorus (P) in a substantial amount are the main compounds for the crystalline structure of Hydroxyapatite. The characterization of materials after adsorption by EDX confirms the retention of lead and cadmium ions (see Figure 3).

Adsorption kinetics behavior

Figure 4 shows the effects of contact time (from 5 min to 120 min) on Sy-HAP and C-HAP for an initial concentrations of the Pb^{2+} and Cd^{2+} ions of 16.5 ppm and 15.4 ppm at ambient temperature

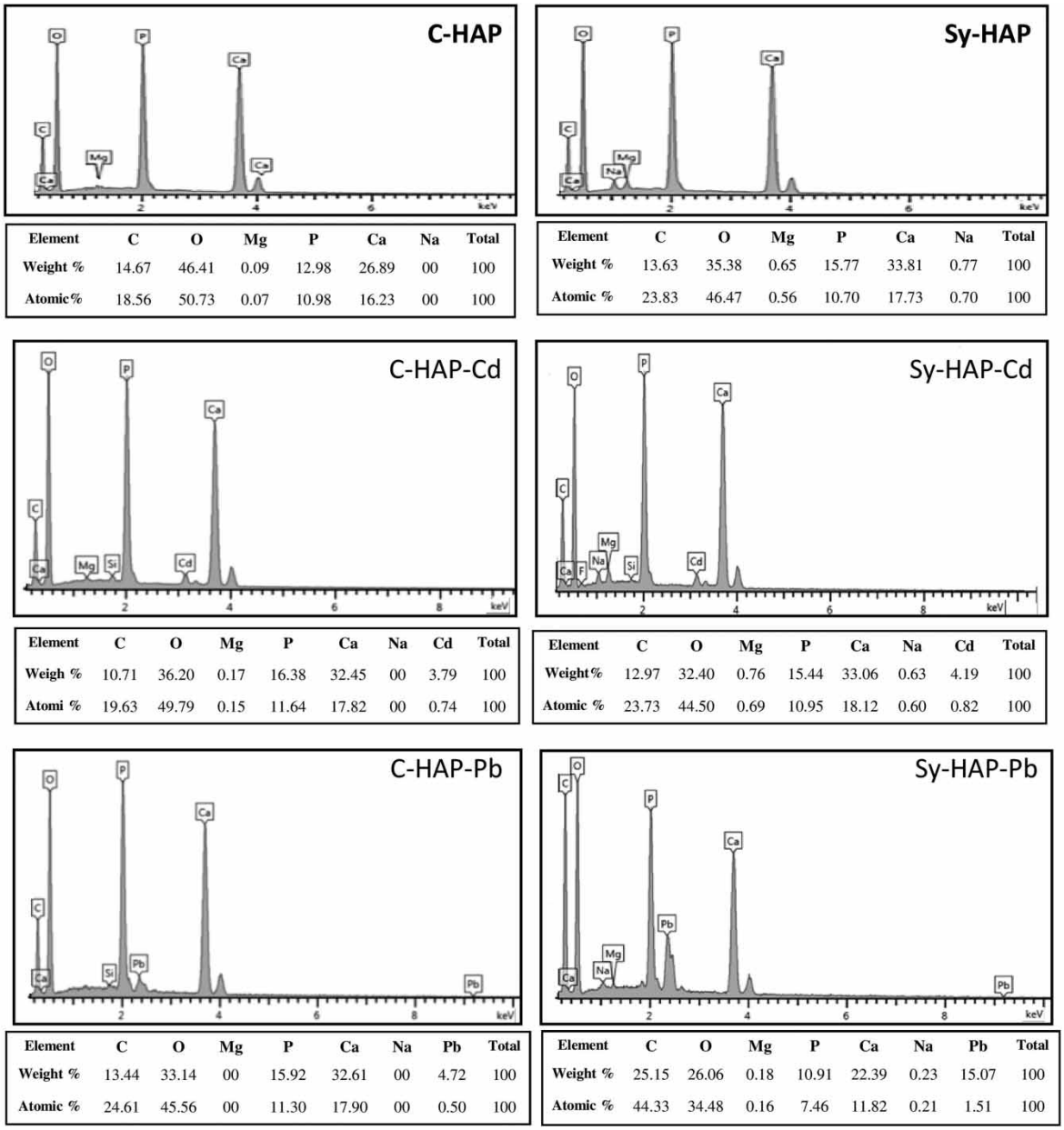

Element	C	O	Mg	P	Ca	Na	Total
Weight %	14.67	46.41	0.09	12.98	26.89	00	100
Atomic%	18.56	50.73	0.07	10.98	16.23	00	100

Element	C	O	Mg	P	Ca	Na	Total
Weight %	13.63	35.38	0.65	15.77	33.81	0.77	100
Atomic %	23.83	46.47	0.56	10.70	17.73	0.70	100

Element	C	O	Mg	P	Ca	Na	Cd	Total
Weigh %	10.71	36.20	0.17	16.38	32.45	00	3.79	100
Atomi %	19.63	49.79	0.15	11.64	17.82	00	0.74	100

Element	C	O	Mg	P	Ca	Na	Cd	Total
Weight%	12.97	32.40	0.76	15.44	33.06	0.63	4.19	100
Atomic %	23.73	44.50	0.69	10.95	18.12	0.60	0.82	100

Element	C	O	Mg	P	Ca	Na	Pb	Total
Weight %	13.44	33.14	00	15.92	32.61	00	4.72	100
Atomic %	24.61	45.56	00	11.30	17.90	00	0.50	100

Element	C	O	Mg	P	Ca	Na	Pb	Total
Weight %	25.15	26.06	0.18	10.91	22.39	0.23	15.07	100
Atomic %	44.33	34.48	0.16	7.46	11.82	0.21	1.51	100

Figure 3 | EDX analysis of hydroxyapatites before and after metal ions adsorption.

Water Practice & Technology Vol 15 No 1
doi: 10.2166/wpt.2020.003

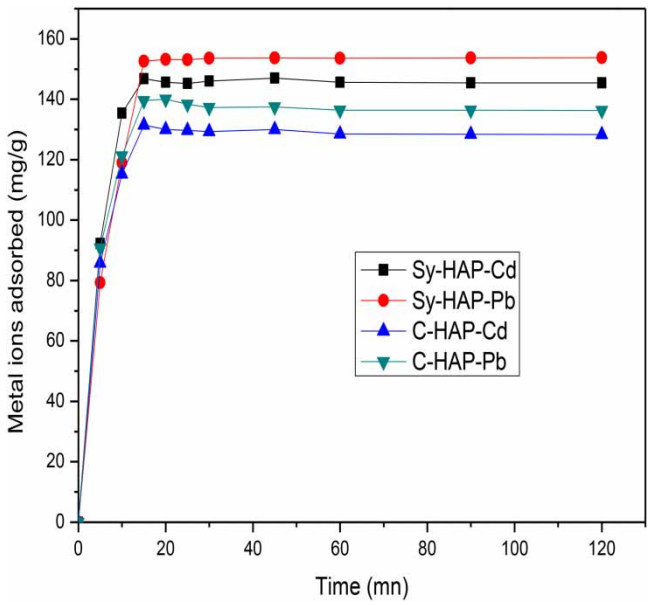

Figure 4 | Effect of contact time.

respectively. It can be observed that the adsorption of cadmium and lead ions increased rapidly with the contact time at the initial stage and reached equilibrium in 15 min for both ions. The removal efficiency of Pb^{2+} is about 86.53% and Cd^{2+} is c.a 81.43% for C-HAP. However; an increase in the removal efficiency was noticed for Sy-HAP; where $Pb^{2+}$and Cd^{2+} ions were removed up to 95.52% and 90.91%, respectively. The maximum adsorbed amounts of lead and cadmium ions onto Sy-HAP are 152.6 mg/g and 139.5 mg/g respectively and whereas, the maximum adsorbed amounts of C-HAP are 146.77 mg/g for Pb^{2+} ions and 131.5 mg/g for Cd^{2+} ions. The trend of the heavy metals removal by Hydroxyapatites therefore follows the order: Pb^{2+} (Sy-HAP) > Cd^{2+} (Sy-HAP) > Pb^{2+} (C-HAP)> Cd^{2+} (C-HAP). The synthetic hydroxyapatite (Sy-HAP) shows higher heavy metals removal efficiency and the adsorption capacity to be in agreement with its higher BET surface area. Jing *et al.* (2018) prepared super-small HA nanoparticles with an average diameter of 7 nm in the presence of glucose as an adsorbent to remove heavy metal ions from wastewater. The maximum adsorption capacities of HA nanoparticles compared to commercial HA to the metal ions are 3,289 mg/g (to Pb^{2+}) and 2,784.8 mg/g (to Cd^{2+}). Jiang *et al.* (2012) used HA hollow microspheres to remove Pb^{2+} and Cd^{2+} mixed ions from water and found that when the initial concentration of the mixed metal ions was 50 μg/mL, the adsorption capacity of Pb^{2+} and Cd^{2+} ions could reach to 99.79 mg/g and 38.78 mg/g, respectively.

Based on the obtained results, the adsorption capacity of Pb^{2+} ion was quite higher than that of cadmium ions. This difference can be attributed to the ionic properties such as ion radius, charge, ionic potential, enthalpy of hydration, electronegativity, and the electron configuration of each metal ion. It is known that, the surface complexation reaction is more influenced by the electrostatic attraction between the surface charge of hydroxyapatite and the dissolved ions (Sönmezay *et al.* 2012; Mousa *et al.* 2016). The electronegativity of Pb^{2+} ion (2.33) is slightly higher than that of Cd^{2+} ion (1.69), which leads to the PbII ion to interact more strongly electrostatically with the surface groups present on the surface of the adsorbent. On the other hand, the tendency to lose water molecules from the aquo-cations is stronger for PbII ion since the single ion hydration enthalpy is −1,481 kJ/mol for PbII ion and −1,807 kJ/mol for CdII ion. This also facilitates the interaction between the PbII ion and the adsorbent surface (Sönmezay *et al.* 2012).

In comparison with the pseudo-first-order model, the linearity of the pseudo-second-order model is good, and the data of R^2 corresponding to various conditions tabulated in Table 1 are above 0.99. In

Water Practice & Technology Vol 15 No 1
doi: 10.2166/wpt.2020.003

Table 1 | Kinetics parameters of $Pb^{2+}$and Cd^{2+} adsorption on the Sy-HAP and C-HAP

Adsorbent/adsorbate		C-HAP Pb^{2+}	C-HAP Cd^{2+}	Sy-HAP Pb^{2+}	Sy-HAP Cd^{2+}
Pseudo-first-order kinetics	K_1 (1/min)	0.308	0.119	0.134	0.106
	q_e (mg/g)	124.45	31,487	78.52	26.79
	R^2	0.659	0.408	0.749	0.6783
Pseudo-second-order kinetics	K_2 (g/(mg min))	0.009	0.008	0.104	0.006
	q_e (mg/g)	3.7129	3.2600	4.0728	2.9520
	R^2	0.999	0.999	0.991	0.99
Intraparticle diffusion	K_d (mg/g $min^{0.5}$)	39.37	36.65	38.93	34.64
	C	2.371	2.941	2.509	2.848
	R^2	0.993	0.989	0.983	0.992

addition, the data of $q_{e,cal}$ derived from the pseudo-second-order model were found to be close to the experimental results, which indicates the appropriateness of this model. Therefore, the pseudo-second-order model can well describe the adsorption kinetics process of metal ions on hydroxyapatites. Furthermore, according to the pseudo-second order model, the boundary layer resistance was not a rate limiting step. For that, the adsorption rate was controlled by intraparticle mass transport in the interior of the adsorbent (Lu *et al.* 2014). According to the experimental results from the representation of the linearized regression Morris and Weber model, the diffusion process occurs within the initial stage (about 15 min). The coefficients of determination are found to be $R^2 = 0.983–0.994$ with $k_d = 34.64–39.37$ (see Table 1). The high R^2 values for this model indicate that the diffusion process occurs fairly well during the initial stage.

Effect of pH

The pH is an important parameter affecting the sorption process. The effect of initial pH on the equilibrium metal cation uptake is given in Figure 5. The cations were adsorbed effectively in the acidic range. Pb^{2+} and Cd^{2+} ions removal was greatly increased by increasing solution *pH* from 2 to 5 for both Sy-HAP and C-HAP. At higher pH values (pH > 5), a slow decrease in the adsorption of metal ions was observed. It is known from literature (Khoo *et al.* 2015; Mousa *et al.* 2016) that

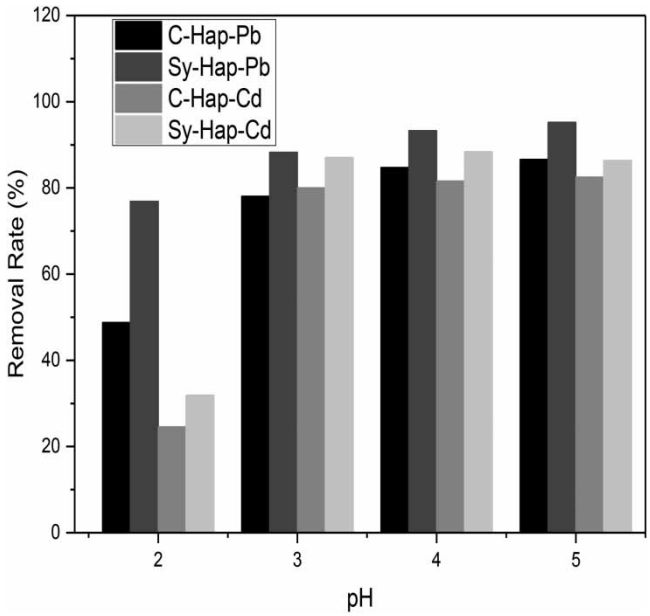

Figure 5 | Effect of pH.

Water Practice & Technology Vol 15 No 1
doi: 10.2166/wpt.2020.003

hydroxyapatites are characterized by the functional groups = PO and = $CaOH_2^+$, which are the predominant sites for a pH value close to the pH_{pzc}. These groups are capable of adsorbing or releasing H^+ ions and they become very significant for a lower pH value and higher than the pH_{pzc}.

At very low pH, the HAP surface would also be surrounded by predominantly H^+ ions. Consequently, repulsive force and the destruction of crystalline structure for the HAP material result in their dissolution in an acidic medium, which results in a decrease in the adsorption of Pb^{2+} and Cd^{2+} ions onto hydroxyapatites (Mousa *et al.* 2016). Furthermore, when the pH increases, the competition between positive charges decreases as these surface active sites become more negatively charged, which increases the adsorption of the Pb^{2+} and Cd^{2+} ions through electrostatic force of attraction (Sönmezay *et al.* 2012; Mousa *et al.* 2016). However, beyond pH 5, no removal increase was observed. The effect of pH has not been studied at higher pH values due to the presence of $PbOH^+$, $Pb(OH)_2$, $[Pb_2(OH)_3]^+$, $[Pb_3(OH)_4]^{2+}$, $[Pb_6(OH)_8]^{4+}$, $Pb(OH)_3$, $CdOH^+$, $Cd(OH)_2$, $Cd(OH)_3^-$ and $Cd(OH)_4^{2-}$ (Sönmezay *et al.* 2012). The formation of these hydroxide species disadvantages the adsorption of Cd^{2+} and Pb^{2+} ions on HAP (Mousa *et al.* 2016). Previous studies have also reported that the best adsorption efficiency of Pb^{2+} and Cd^{2+} ions has been observed at pH 4 and 5 (Sönmezay *et al.* 2012; Mousa *et al.* 2016). On the other hand, pH can have a substantial influence on the surface charge of solids, which behaved differently in adsorbing metal ions at different solution pHs. The pH_{pzc} of Sy-HAP and C-HAP powders was found to be 5.8 and 4.6 respectively. This means that the HAP surface was positively charged at solution pH below pH_{pzc} and Pb^{2+} ions were repulsed by the HAP material surface, resulting in the removal of Cd^{2+} and Pb^{2+} ions. At pH higher than pH_{pzc}, the surface of HAP can be deprotonated and typically charges negatively (Herbache *et al.* 2016; Mousa *et al.* 2016). Thus, it is advantageous that the process is a suitable application for heavy metals removal because of its neutral and clean effluent.

Adsorption isotherm behavior

Figure 6 shows that the metal adsorption capacity of both biomaterials increased gradually with the adsorption concentration at equilibrium. The Sy-HAP presents the highest rate of adsorption for both metallic ions. For different heavy metal ions, at low initial concentrations, the adsorption equilibrium is quickly reached and saturation is achieved; while with high initial concentrations, the adsorption is

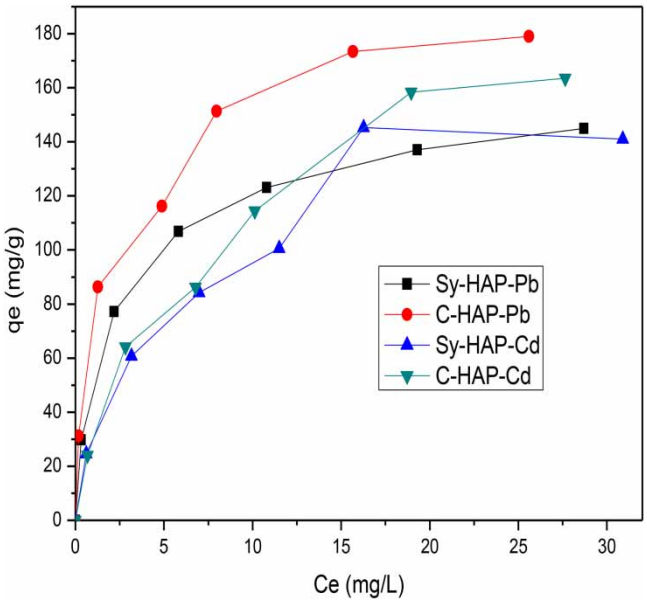

Figure 6 | Effect of initial concentration.

Water Practice & Technology Vol 15 No 1
doi: 10.2166/wpt.2020.003

slow and the driving force greater, forcing the solution to reach equilibrium easier. This indicates that HAP has a high affinity for the metals studied. Furthermore, the maximum adsorption is achieved with an adsorption capacity in the order of 166.67 mg/g Pb^{2+} ion, 138.89 mg/g Cd^{2+} ion, 142.86 mg/g Pb^{2+} ion and 125 mg/g Cd^{2+} ion for Sy-HAP and C-HAP, respectively. The parameters and coefficient of determination (R^2) obtained are reported in Table 2. It can be concluded that the Langmuir, Freundlich and Temkin models are the most valid to describe and evaluate the adsorption processes for the Pb^{2+} and Cd^{2+} ion adsorption by the HAP material. Whereas the Dubinin – Radushkevich (D – R) model was found to be less favorable for elucidating these types of surface reactions. The validity of the isotherm models is in the following order (Table 2), Langmuir, Freundlich and Temkin > Dubinin-Radushkevich. Based on the slight difference in R^2 values, which exceed 0.984, and based on the pore size of both materials, which belong to mesoporous materials, the appropriate model should be Freundlich.

Table 2 | Adsorption isotherm models for the adsorption of Pb^{2+} and Cd^{2+} onto Sy-HAP and C-HAP

Adsorbate		Pb^{2+}		Cd^{2+}	
Adsorbent		C-HAP	Sy-HAP	C-HAP	Sy-HAP
Freundlich	K_F	0.231	0.259	0.181	0.118
	1/n	0.328	0.363	0.451	0.535
	R^2	0.996	0.963	0.991	0.986
Langmuir	K_L	0.875	1.502	0.4	0.3
	q_m	142.86	166.67	125	138.89
	q_t	142.77	152.75	131.5	140
	R^2	0.984	0.986	0.989	0.992
Temkin	B	28.44	32.6	30.06	14.23
	b_T	87.074	76.96	82.38	174.02
	K_T	0.716	0.91	0.072	1.149
	R^2	0.986	0.984	0.974	0.97
Dubinin-Radushkevich	K_D	$5.256*10^{-5}$	$6.765*10^{-5}$	$1.4523*10^{-5}$	$1.165*10^{-5}$
	q_{mDR}	122.76	1,432.643	112. 678	124.328
	R^2	0.86	0.882	0.826	0.945

Thermodynamic parameters

The values of standard enthalpy and entropy of the adsorption can be determined from the slope and intercept of a linear plot of ln K_d vs 1/T. The calculated values of the thermodynamic data are shown in Table 3. The overall lead and cadmium adsorption process seems to be endothermic (ΔH_{ads} Pb^{2+} (C-HAP) = 32.093 kJ/K*mol, ΔH_{ads} Pb^{2+} (Sy-HAP) = 14.783 kJ/K*mol, ΔH_{ads} Cd^{2+} (C-HAP) = 22.57 kJ/K*mol, and ΔH_{ads} Cd^{2+} (Sy-HAP) = 6.922 kJ/K*mol). Although not very high, these values of enthalpy ΔH_{ads} can be interpreted on the basis of considerably strong interaction between

Table 3 | Thermodynamic parameters for the adsorption of Pb^{2+} and Cd^{2+} onto Sy-HAP and C-HAP

			$-(\Delta G_{ads})$ (KJ/K.mol)			
	ΔH_{ads} (KJ/K.mol)	ΔS_{ads} (KJ/mol)	293	303	313	323
Pb^{2+} (C-HAP)	32.09	0.14	9.80	11.2	12.66	14.12
Pb^{2+} (Sy-HAP)	14.783	0.079	8.36	9.15	9.94	10.73
Cd^{2+} (C-HAP)	22.57	0.115	11.12	12.27	13.42	14.57
Cd^{2+} (Sy-HAP)	6.922	0.059	10.36	10.95	11.54	12.14

Water Practice & Technology Vol 15 No 1
doi: 10.2166/wpt.2020.003

metal ions and hydroxyapatite surface under ion exchange process. Negative values of free energy ΔG_{ads} (−14.575 to −8.364 kJ/K*mol) confirm the spontaneous nature of the adsorption. Also, it can be noticed that for different adsorbents, ΔG_{ads} increases with the increase in the solution temperature. Indeed, the ΔS_{ads} values were positive (0.012–0.056 kJ/mol). This occurs as a result of redistribution of energy and an increased randomness at the adsorbent– adsorbate interface during the adsorption process. Similar observations were reported for the adsorption of lead and cadmium ions from aqueous solution onto different materials such as Schiff base-modified nanoparticles, amino-bacterial cellulose, modified biomass ash and manganese oxide minerals (Sönmezay *et al.* 2012; Lu *et al.* 2014; Herbache *et al.* 2016; Xu *et al.* 2017).

CONCLUSION

Adsorption performance of a low-cost and efficient adsorbent prepared from bovine bones, Sy-HAP, was studied for the removal of Pb^{2+} and Cd^{2+} ions from aqueous solutions, compared to commercial hydroxyapatite C-HAP. The experimental results indicated that the equilibrium time required for a maximum adsorption of Pb^{2+} and Cd^{2+} ions on both hydroxyapatites is 15 min. The obtained yields for Sy-HAP are 96.52% and 92.91% for Pb^{2+} and Cd^{2+} ions respectively, whereas C-HAP presents slightly lower removal efficiencies of 87.53% and 85.43% for Pb^{2+} and Cd^{2+} respectively. These removal efficiencies correspond to the maximal adsorption capacities of Pb^{2+} 152.6 mg/g and Cd^{2+} 139.5 mg/g, respectively for Sy-HAP and to Pb^{2+} 138.77 mg/g and Cd^{2+} 131.5 mg/g, respectively for C-HAP. The best adsorption efficiency of Pb^{2+} and Cd^{2+} ions has been observed at pH 5 for both hydroxyapatites. Isotherm adsorption studies indicated that Langmuir, Freundlich and Temkin are the most valid models to describe and evaluate the adsorption process. Indeed, the kinetic adsorption process followed the pseudo-second-order with intraparticle diffusion, which is significant at the initial adsorption stage. Negative values of ΔG_{ads} and positive values of ΔH_{ads} indicate that the adsorption process is spontaneous and endothermic with a physical nature. The results show that efficient and inexpensive hydroxyapatite minerals can be useful adsorbents for removing metal ions from aqueous solution.

ACKNOWLEDGEMENTS

The author would like to thank the European Institute of Membranes, University Montpellier, France, for the realization of characterization of materials in this present study.

REFERENCES

Alexander, J. A., Surajudeen, A., Aliyu, E. U., Omeiza, A. O. & Zaini, M. A. A. 2017 Multi-metals column adsorption of lead(II), cadmium(II) and manganese(II) onto natural bentonite clay. *Water Sci. Technol.* **76**(8), 2232–2241.

Ben-Arfa, B. A. E., Salvado, I. M. M., Ferreira, J. M. F. & Pullar, R. C. 2017 Novel route for rapid sol-gel synthesis of hydroxyapatite, avoiding ageing and using fast drying with a 50-fold to 200-fold reduction in process time. *Mater. Sci. Eng., C.* **70**, 796–804.

Cengiz, B., Gokce, Y., Yildiz, N., Aktas, Z. & Calimli, A. 2008 Synthesis and characterization of hydroxyapatite nanoparticles. *Colloid Surf., A: Physicochem Eng. Asp.* **322**, 29–33.

França de Oliveira, D., Mendes Neri, J. A., Alves de Almeida Ribeiro, J., Soares dos Santos, F. & Kister de Pietre, M. 2017 Synthesis of zeolites with different chemical and textural properties for metal ions removal from aqueous solutions. *Water Sci. Technol.* **76**(12), 3441–3451.

Herbache, H., Ramdani, A., Maghni, A., Taleb, Z., Taleb, S., Morallon, E. & Brahmi, R. 2016 Removal of o-Cresol from aqueous solution using Algerian Na-Clay as adsorbent. *Desalin. Water Treat.* **57**, 20511–20519.

Jiang, S. D., Yao, A. Z., Zhou, Q. T. & Fu, S. Q. 2012 Fabrication of hydroxyapatite hierarchical hollow microspheres and potential application in water treatment. *J. Phys. Chem. C.* **116**, 4484–4492.

Water Practice & Technology Vol 15 No 1
doi: 10.2166/wpt.2020.003

Jing, N., Zhou, A. N. & Xu, Q. H. 2018 The synthesis of super-small nano hydroxyapatite and its high adsorptions to mixed heavy metallic ions. *J. Hazard. Mater.* **353**, 89–98.

Kemençe, N. & Bölgen, N. 2017 Gelatin- and hydroxyapatite-based cryogels for bone tissue engineering: synthesis, characterization, in vitro and in vivo biocompatibility. *J. Tissue Eng. Regener Med.* **11**, 20–33.

Khoo, W., Nor, F. M., Ardhyananta, H. & Kurniawan, D. 2015 Preparation of natural hydroxyapatite from bovine femur bones using calcination at various temperatures. *Procedia Manuf.* **2**, 196–201.

Kim, J., Lee, J. & Kim, H. 2016 Hydroxyapatite mineral tubes developed for the loading and release of biological proteins. *Mater. Lett.* **167**, 170–174.

Kołodyńska, D., Krukowska-Bąka, J., Kazmierczak-Razna, J. & Pietrzak, R. 2017 Uptake of heavy metal ions from aqueous solutions by sorbents obtained from the spent ion exchange resins. *Microporous Mesoporous Mater.* **244**, 127–136.

Li, W., Liao, X., Wang, L. & Huang, Z. 2019 Adsorption of cadmium and lead in wastewater by four kinds of biomass xanthates. *Water Sci. Technol.* **79**(6), 1222–1230.

Lu, M., Zhang, Y. M., Guan, X. H., Xu, X. H. & Gao, T. T. 2014 Thermodynamics and kinetics of adsorption for heavy metal ions from aqueous solutions onto surface amino-bacterial cellulose. *Trans. Nonferrous Met. Soc. China* **24**, 1912–1917.

Moftakhar, M. K., Yaftian, M. R. & Ghorbanloo, M. 2016 Schiff base-modified nanoparticles for removal of heavy metals, adsorption efficiency, thermodynamics and kinetics of Schiff base-modified nanoparticles for removal of heavy metals. *Int. J. Environ. Sci. Technol.* **13**, 1707–1722.

Mousa, S. M., Ammar, N. S. & Ibrahim, H. A. 2016 Removal of lead ions using hydroxyapatite nano-material prepared from phosphogypsum waste. *J. Saudi Chem. Soc.* **20**(3), 357–365.

Murakami, S. 1981 Semi-xylenol orange complexes with bivalent metal ions. *J. Inorg. Nucl. Chem.* **43**, 335–343.

Official Journal of the Algerian Republic N°18 2011 *Quality Parameters of Human Consumption Water*. Algiers, Algeria.

Official Journal of the Algerian Republic N°26 2006 *Standards and Limit Values of the Discharge Parameters of Industrial Liquid Effluents*. Algiers, Algeria.

Pobi, K. K., Mondal, B., Nayek, S., Patra, A. K. & Saha, R. 2019 Efficient removal of Hg^{2+}, Cd^{2+} and Pb^{2+} from aqueous solution and mixed industrial wastewater using a designed chelating ligand, 2-pyridyl-N-(2′-methylthiophenyl) methyleneimine (PMTPM). *Water Sci. Technol.* **79**(6), 1092–1101.

Song, Y., Gao, J., Zhang, Y. & Song, S. 2016 Preparation and characterization of nano-hydroxyapatite and its competitive adsorption kinetics of copper and lead ions in water. *Nanomater. Nanotechnol.* **6**, 1–8.

Sönmezay, A., Öncel, M. S. & Bektaŝ, N. 2012 Adsorption of lead and cadmium ions from aqueous solutions using manganoxide minerals. *Trans. Nonferrous Met. Soc. China* **22**, 3131–3313.

Ullah, I., Abbas, A., Al-Amer, A. M., Laoui, T., Al-Marri, M. J., Nasser, M. S., Khraisheh, M. & Atieh, M. A. 2016 Heavy metal removal from aqueous solution by advanced carbon nanotubes: critical review of adsorption applications. *Sep. Purif. Technol.* **157**, 141–161.

WHO 1993 *Guidelines for Drinking-Water Quality*, 2nd edn. World Health Organization, Geneva, Switzerland.

Xu, L., Zheng, X., Cui, H., Zhu, Z., Liang, J. & Zhou, J. 2017 Equilibrium, kinetic, and thermodynamic studies on the adsorption of cadmium from aqueous solution by modified biomass Ash. *Bioinorg. Chem. Appl.* **12**, 1–9.

Yan, J., Miao, Y., Tan, H., Zhou, T., Ling, Z., Chen, Y., Xing, X. & Hu, X. 2016 Injectable alginate/hydroxyapatite gel scaffold combined with gelatin microspheres for drug delivery and bone tissue engineering. *Mater. Sci. Eng. C.* **63**, 274–284.

Zhao, J., Liu, Y., Sun, W. & Yang, X. 2012 First detection, characterization, and application of amorphous calcium phosphate in dentistry. *J. Dent. Sci.* **7**, 316–323.